Virchows Arch (2016) 468:741–755
DOI 10.1007/s00428-016-1926-9

ORIGINAL ARTICLE

Giant cell rich osteosarcoma revisited—diagnostic criteria and histopathologic patterns, Ki67, CDK4, and MDM2 expression, changes in response to bisphosphonate and denosumab treatment

Louis Tsun Cheung Chow[1]

Received: 4 December 2015 / Revised: 1 March 2016 / Accepted: 8 March 2016 / Published online: 22 March 2016

Abstract Defining giant cell-rich osteosarcoma (GCRO) as "an osteosarcoma in which more than 50% of the tumor consists of numerous uniformly distributed osteoclastic giant cells amidst oval or spindle mononuclear cells embedded in a fibrovascular stroma," eight such cases identified among 265 cases of osteosarcoma were analysed. Their age ranges from 11 to 33 years, with peak incidence in the second decade and equal sex distribution. Seventy-five percent presented with pain, commonest in the knee, affecting the metaphysis. Most appeared radiologically as well-circumscribed expansile multiloculated osteolytic lesions, and many are displayed periosteal reaction. They showed several distinct histologic patterns: the stromal and giant cell, fibrohistiocytic, aneurysmal-cystic, osteoblastoma-like, and parosteal and fibrous dysplasia-like patterns. Focal subtle lacelike osteoid deposition, permeative infiltration into adjacent native bony trabeculae and over 30 % Ki67 proliferative index were characteristic. There was no CDK4 and MDM2 amplification. In those having bisphosphonate and denosumab treatment, there was limited focal necrosis with reduction in the number of giant cells and broad trabecular woven bone formation but no giant osteoclast was seen. Two patients with initial diagnosis of giant cell tumor treated by curettage and local resection pursued aggressive clinical courses, died after 14 and 21 months. The others survived 12 to 110 months. GCRO accounts for about 3 % of all osteosarcomas and apart from its more frequent diaphyseal location and associated normal bone-specific alkaline phosphate levels; it shares with conventional high-grade osteosarcoma the same patient demographics, sites of occurrence, absence of CDK4 and MDM2 amplification, and probably clinical course.

Keywords Giant cell rich osteosarcoma · Osteosarcoma · Giant cell tumor · Telangiectatic osteosarcoma · Bisphosphonate · Denosumab

✉ Louis Tsun Cheung Chow
louistcchow@gmail.com

[1] Department of Anatomical and Cellular Pathology, Prince of Wales Hospital, 30-32 Ngan Shing Street, Shatin, Hong Kong, China

Introduction

Osteosarcoma is subdivided histopathologically into osteoblastic, chondroblastic, or fibroblastic, division arbitrarily taken to indicate greater than 50 % prevalence of that particular histologic type; uncommon variants include giant cell-rich, osteoblastoma-like, epithelioid, and small-cell subtypes [1]. Giant cell rich osteosarcoma (GCRO), first described by Bathurst, is characterized by an abundance of osteoclastic giant cells and paucity of tumor osteoid [2], leading to its confusion with giant cell tumor (GCT) [3], especially when it adopts an epiphyseal location [4]. It constitutes about 3 % of osteosarcomas [2, 5] and is included in the WHO classification of bone tumors [6].

GCRO mimics GCT radiologically; Bathurst states "many of the classical radiological features of an osteosarcoma are absent in these cases and differentiation from a benign lesion is sometimes difficult" [2]. Four of Bathurst's nine cases are considered radiologically benign. Six of Wang's nine cases are diagnosed radiologically as GCT; two are 13 and 15 years of age [5]. Whereas it appears imprudent to render a diagnosis of GCT in the skeletally immature, one should note that 1.8–5.7 % of GCT occurs in patients of that age range [7–9]; 30.8 % of them affects exclusively the metaphysis [7]. Thus, though GCT rarely affects the skeletally immature and seldom occurs solely in the metaphysis, for those affecting the skeletally immature, GCT is often exclusively metaphyseal, posing further difficulties in its differentiation from GCRO.

About 35 cases of GCRO have been reported in the English literature [2–5, 10–24]; the exact histologic criteria for diagnosis and histopathologic spectrum have never been clearly defined. Short of precise defining criteria, characterization of the clinical, radiologic, and pathologic features is difficult. For instance, its position in the spectrum of low to high-grade osteosarcoma is uncertain since there are GCRO showing radiologic, gross, and histopathologic features typical of parosteal osteosarcoma [10], GCRO resulting from dedifferentiated parosteal osteosarcoma [12] and the author's report of GCRO virtually indistinguishable radiologically and histologically from GCT yet pursuing an aggressively fatal outcome [3]. Study of the status of cyclin-dependent kinase 4 (CDK4) and mouse double minute 2 (MDM2) expression may be helpful as their amplification is seen in 89 % of low grade fibrous dysplasia-like and parosteal osteosarcoma [25], areas of which are present in high-grade osteosarcoma, indicating probable dedifferentiation [26]. Moreover, a high Ki67 proliferative index of over 20 % in GCRO is found to be useful in its differentiation from GCT [3]. With unifying diagnostic criteria for GCRO, these ancillary measures may be applied for its proper placement into the family osteosarcoma.

The present investigation aims at filling these deficiencies in the knowledge of GCRO, notably its definition and various clinical and histopathologic attributes. In accordance with the conventional histologic classification of osteosarcoma, GCRO is defined as "*an osteosarcoma in which more than 50% of the tumor consists of numerous uniformly distributed osteoclastic giant cells amidst oval or spindle mononuclear cells embedded in a fibrovascular stroma*."

Applying such definition, we describe eight patients with GCRO, six masquerading radiographically as GCT, and their distinction from GCRO has been impossible even on needle biopsy in two [3, 4]. Two patients received bisphosphonate and denosumab, one mere bisphosphonate treatment prior to resection of the tumor either because of the initial impression of GCT, or in an empirical attempt to consolidate the tumor. The clinical, radiologic, and histopathologic features of these eight patients are analyzed with emphasis on the background histomorphologic features accompanying the giant cell-rich pattern and the changes after bisphosphonate and denosumab treatment. The Ki67 proliferative index, CDK4, and MDM2 amplification status are studied by immunohistochemistry and fluorescence in situ hybridization (FISH) to help in the assignment of GCRO into the proper grade in the osteosarcoma family. Finally, the English literation on all GCRO cases was reviewed.

Materials and methods

The clinical records, radiological images, and pathological materials from 265 cases of histologically proven osteosarcoma in our hospital between January 1985 and October 2015 were studied. Eight fulfilled our diagnostic criteria for GCRO. In all cases, the entire tumor was embedded. For immunohistochemical studies, avidin-biotin complex was used as the detection system after microwave antigen retrieval. Automated immunostaining employed the Ventana Ultraview detection kit and Benchmark XT staining system with appropriate positive and negative controls. To evaluate the staining intensity for Ki-67 {SP6, dilution 1:400, ThermoSci (RM-9106S), Fremont, CA,USA}, positive cells were counted among 500 randomly selected tumor cells.

CKD4 and MDM2 amplification was studied by immunohistochemistry and FISH. For immunohistochemistry, only nuclear stains of neoplastic cells were considered as positive. For CDK4 (mouse monoclonal antibody clone DCS-31, dilution 1:200; Invitrogen) and MDM2 (mouse monoclonal antibody clone IF2, 1:50 dilution; Invitrogen, Carlsbad, CA), the number of positive cells were counted among 500 randomly selected tumor cells. Intensity of staining was semi-quantitatively graded: 0, negative; 1+, weak-positive; 2+, moderate-positive; and 3+, strong-positive. Extent of staining was classified as 0 to less than 1 % (negative), 1 to 10 % (focal), and greater than 10 to 100 % (diffuse). For FISH, the SPEC CDK4/CEN12 and MDM2/CEN12 Dual Color Probe (ZytoVision GmbH, Bremerhaven, Germany) was applied according to the manufacturer's protocol. The tumors were scored by counting a minimum of 100 tumor cell nuclei at 100 magnifications. The number of CDK4 and MDM2 and CEN 12 signals was determined, and the CDK4 and MDM2/CEN 12 ratio was calculated for each nucleus. A ratio greater than 2.5 and 2.0 in at least 10 % of nuclei was considered amplified for the CDK4 and MDM2 gene, respectively.

Results

Clinical and radiologic features

The clinical and radiologic features are summarized in Table 1. Our eight patients ranged in age from 11 to 33 years, with peak incidence in the second decade and equal sex distribution. Six (75 %) presented with pain with or without detectable swellings for a few weeks to months, one (12.5 %) with pathologic fracture, one (12.5 %) with a painless enlarging mass for 2 years. All recalled no preceding trauma.

The lesions were commonly in the knee, three (37.5 %) in distal femur, two (25 %) proximal tibia, and one (12.5 %) in proximal fibula. Two (25 %) affected the metatarsal. In the long bones, all except one involved the metaphysis with variable epiphyseal extension and the last one epiphyseal in location. On plain radiography, all appeared as expansile osteolytic lesions with cortical erosion; the majority were multiloculated (87.5 %) and 5 (62.5 %) demonstrated periosteal reaction (Figs. 1, 2, and 3). None showed any osteoblastic areas.

Table 1 Summary of the clinical and radiologic features of our patients with giant cell rich osteosarcoma

Patient sex/age	Symptoms	Plain radiographic features	Radiological DDx	Needle biopsy DDx	Treatment	Outcome
1 M/16	Left knee pain for 3 weeks	• Well-defined multiloculated expansile osteolytic lesion; Left tibia proximal epiphysis and metaphysis	• GCT • Chondroblastoma • Osteosarcoma	• GCRO	Above knee amputation (skip metastasis in left lower femur) followed by chemotherapy	Well 110 months, NED
2 F/26	Increasing right knee pain for a few months	• Subarticular well-defined expansile multiloculated osteolytic lesion; Right femur distal epiphysis	• GCT	• GCT	**Bisphosphonate**; Curettage (diagnosis of GCRO made); above knee amputation and chemotherapy	Died 14 months widespread metastases
3 M/12	Painful enlarging firm mass left upper leg for a few weeks	• Well-defined multiloculated expansile osteolytic lesion, periosteal reaction in inferior aspect; Left fibula proximal metaphysis	• GCT • Chondroblastoma • Osteosarcoma	• GCT • GCRO • Telangiectatic Osteosarcoma	Excision of fibular tumor, local recurrence; thigh and groin lymph node metastasis, diagnosis of GCRO; **Bisphosphonate** and **Denosumab**; Disarticulation, chemotherapy	Died 21 months widespread metastases
4 F/33	Increasing painful swelling right knee for 2 months	• Infiltrative expansile osteolytic lesion; cortical erosion, periosteal reaction, Right femur distal meta-epiphysis	• Osteosarcoma	• GCRO	Chemotherapy followed by resection	Well 48 months, NED
5 F/15	Left knee pain for a few months	• Well-defined multiloculated expansile osteolytic lesion, ground glass matrix, streaky bone formation, periosteal reaction; Left proximal tibial meta-epiphysis	• GCT • ABC	• GCRO	Chemotherapy followed by resection	Well 38 months, NED
6 F/31	Slowly enlarging mass right foot for 2 years	• Well-defined multiloculated expansile osteolytic lesion replacing almost the entire first metatarsal right foot	• GCT	• GCRO	**Bisphosphonate** and **Denosumab**; Ray amputation of big toe and first metatarsal; chemotherapy	Solitary iliac metastasis after 1 year, resected Well 30 months, NED
7 M/11	Well all along; pain from pathological fracture after right ankle sprain	• Fairly well-defined expansile osteolytic lesion, cortical erosion, periosteal reaction; Right 4th metatarsal diaphysis	• Osteosarcoma • Fibrous dysplasia	• Osteoblastoma-like osteosarcoma	Chemotherapy followed by resection	Well 21 months, NED
8 M/15	Right knee painful swelling 2 months	• Well-defined multiloculated expansile osteolytic lesion, thin rim of sclerosis, periosteal reaction; Right distal femur	• GCT/CB with ABC • Telangiectatic Osteosarcoma	• GCRO	Chemotherapy followed by resection	Well 12 months, NED

DDx differential diagnosis, *GCT* giant cell tumor, *GCRO* giant cell rich osteosarcoma, *ABC* aneurysmal bone cyst, *CB* chondroblastoma, *NED* no evidence of disease

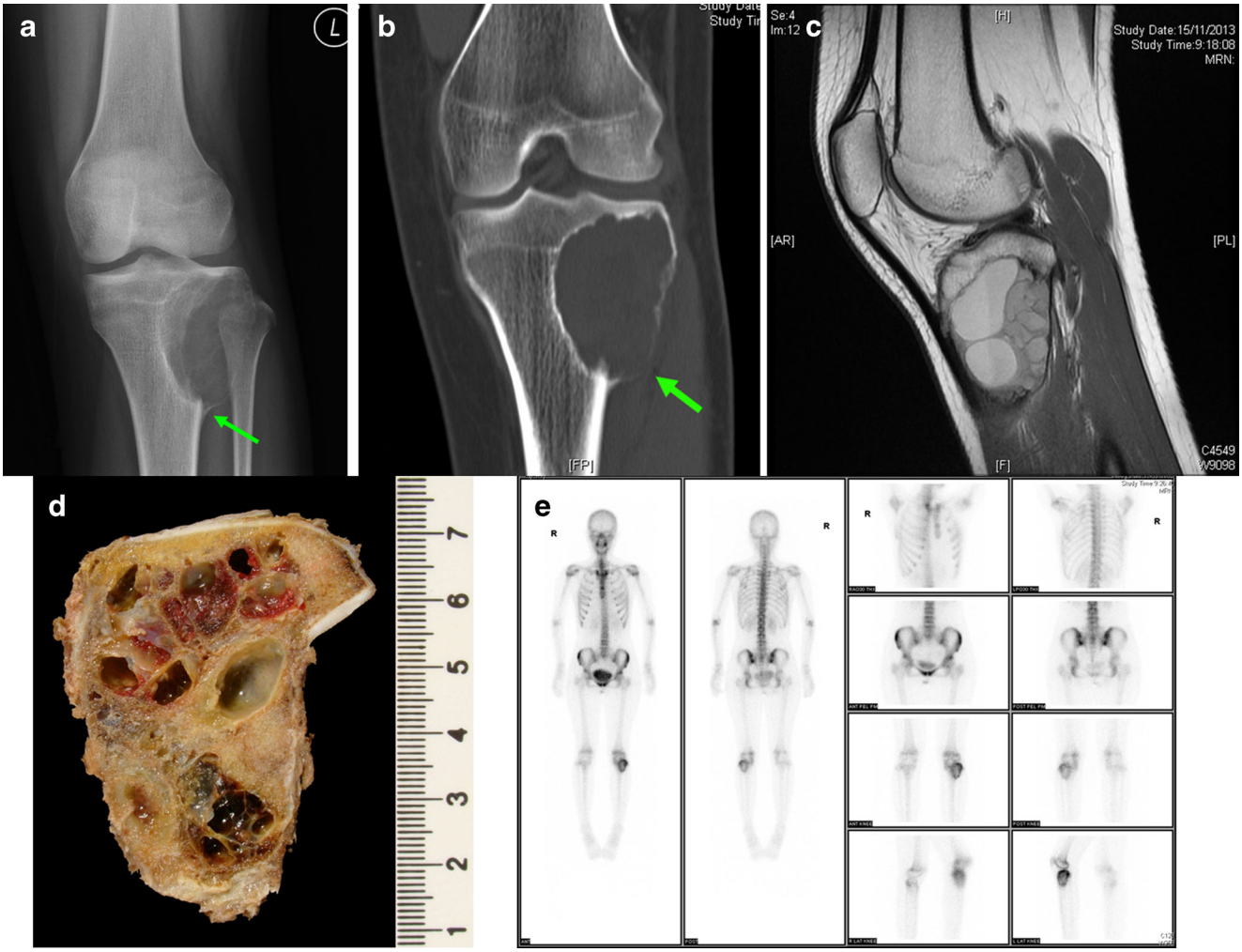

Fig. 1 **a** Plain radiograph of patient 5 showing an expansile multiloculated osteolytic lesion in the metaphyseal region of the left tibia. The border of the lesion is fairly well demarcated but periosteal reaction is noted in its inferior aspect (*arrow*). **b** Computerized tomograph (CT) of patient 5 showing the well circumscription and osteolytic nature of the lesion. There is focal cortical erosion and probable soft tissue extension (*arrow*). No osteoblastic area seen within the tumor. **c** Magnetic resonance imaging (MRI) of patient 5 showing mixed hyperintense and hypointense T1-weighted signals with prominent multiloculation. **d** Cut section of the resected tumor of patient 5 showing light yellowish brown firm tissue with prominent multiloculated cystic changes. **e** Bone scan of patient 5 showing increased uptake in the left tibial tumor

CT and MRI demonstrated their osteolytic nature with variable cortical erosion and soft tissue extension (Fig. 1b). Most appeared as mixed hyperintense and hypointense signals on T1-weighted and inhomogeneous hyperintense signals on T2-weighted images. In five (62.5 %), internal septa with multiloculations and multiple fluid levels were noted (Figs. 1c, 2b, and 3b). They showed no osteoblastic areas but demonstrated increased radioactive uptake on bone scan (Fig. 1e).

Biochemical findings and gross pathology (Table 2)

The serum calcium, phosphate, and bone-specific alkaline phosphatase in all patients were within normal range for their age. The tumors of showed light brown or pale gray firm cut surfaces with varying degrees of multiloculation or cystic change, hemorrhage, and necrosis (Fig. 1d, 2c, and 3c). Cortical erosion was seen in all and extension into surrounding soft tissue was noted in three (patients 1, 2, and 6). In four (1, 3, 5, and 8), the tumor showed prominent multiloculations or cystic changes. The cysts consisted of thin fibrous wall and contained brownish serosanguineous fluid, sometimes with brownish granular friable tissue adherent on their surfaces, producing an aneurysmal cystic appearance (Figs. 1d and 3c).

Histopathology

The tumors showed several histopathologic patterns in varying combinations and proportions. In descending

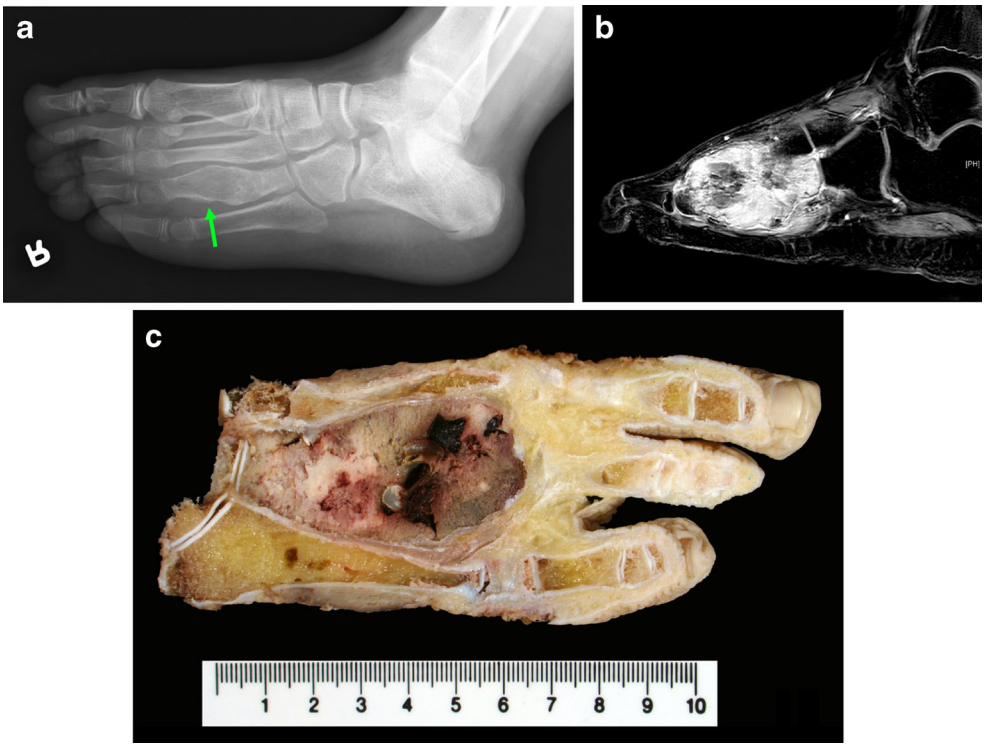

Fig. 2 **a** Plain radiograph of patient 7 showing an expansile multiloculated osteolytic lesion in the right fourth metatarsal with focal cortical erosion and periosteal reaction (*arrow*). **b** MRI of patient 7. The multiloculated tumor shows inhomogeneous hyperintense T2-weighted signals with replacement of almost the entire metatarsal and cortical erosion. **c** Cut section of the resected tumor of patient 7 showing light yellowish brown firm tissue with focal necrosis and hemorrhage

order of prevalence, they included the stromal and giant cell, fibrohistiocytic, aneurysmal-cystic, osteoblastoma-like, and parosteal and fibrous dysplasia-like patterns. Areas of necrosis were seen especially in those with pre-operative chemotherapy. All showed focal permeative infiltration into surrounding native bony trabeculae; lymphovascular permeation was detected in three (2, 3, and 4).

Stromal and giant cell pattern

The stromal and giant cell pattern consisted of abundant evenly distributed osteoclastic giant cells amidst oval or spindle mononuclear cells supported in a fibrovascular stroma (Fig. 4). Most stromal cells showed mild nuclear pleomorphism and infrequent mitosis but, focally, they possessed moderately to markedly pleomorphic nuclei; some showed

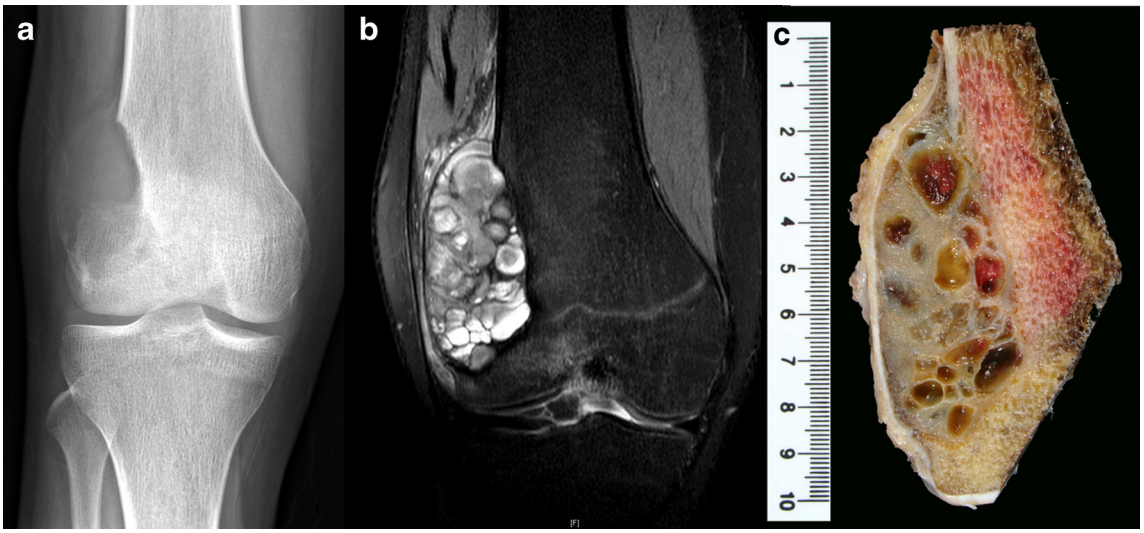

Fig. 3 **a** Plain radiograph of patient 8 showing an expansile multiloculated osteolytic lesion in the metaphyseal region of the left distal femur. The border of the lesion is fairly well demarcated. **b** MRI of patient 8 showing inhomogeneous hyperintense T2-weighted signals with prominent multiloculations. **c** Cut section of the resected tumor from patient 8 showing pale gray firm to hard tissue with prominent cystic changes. The tumor erodes through the cortex and elevates the periosteum (superior aspect of tumor)

Table 2 Summary of the biochemical and pathologic features of our patients with giant cell rich osteosarcoma

Patient sex/ age	Biochemical findings	Needle biopsy features	Resected specimen gross pathology	Resected specimen histopathology	Immunohistochemistry molecular study
1 M/16	• Ca: 2.38 • PO_4: 1.4 • AP: 93	• Stromal and giant cell pattern • Moderate stromal cell nuclear pleomorphism, atypical mitosis • Lace-like osteoid deposition	• Light brown soft to firm tibial tumor 5 × 6 × 13 cm with prominent hemorrhagic cystic changes, invading through cortex to soft tissue and fibula • Femur skip metastatic hemorrhagic nodule 1 cm	• Stromal and giant cell pattern 55 % • Aneurysmal cystic pattern 35 % • Fibrohistiocytic pattern 10 %	• Ki 67: 33 %
2 F/26	• Ca: 2.31 • PO_4: 0.98 • AP: 61	• Fibrohistiocytic pattern with scattered giant cell, mild nuclear pleomorphism, no mitosis, no osteoid deposition	• Light brown firm right distal femur tumor 7 × 9 × 15 cm with only focal small areas of hemorrhagic cystic changes, invading through cortex to knee joint, skeletal muscle, and soft tissue	• Stromal and giant cell pattern 85 % in curettage, 70 % in resected tumor • Fibrohistiocytic pattern 30 % • Lymphovascular permeation	• Ki67 38 % • FISH for CDK4 –ve • FISH for MDM2 -ve
3 M/12	• Ca: 2.33 • PO_4: 1.35 • AP: 261	• Stromal and giant cell pattern • Moderate stromal cell nuclear pleomorphism • Lace-like osteoid deposition	• Light brown soft to firm left proximal fibular tumor 4 × 4.5 × 8 cm with prominent hemorrhagic cystic changes, tumor largely confined to fibula	• Stromal and giant cell pattern 70 % • Aneurysmal cystic pattern 25 % • Fibrohistiocytic pattern 5 % • Lymphovascular permeation	• Ki67: 34 % • FISH for CDK4 –ve • FISH for MDM2 -ve
4 F/33	• Ca: 2.35 • PO_4: 1.3 • AP: 75	• Stromal and giant cell pattern • Moderate stromal cell nuclear pleomorphism, atypical mitosis • Subtle small irregular osteoid	• Brownish red friable tumor 5 × 6 × 7, left inferior femoral metaphysis with small focal necrosis and hemorrhage; focal cortical erosion	• Stromal and giant cell pattern 80 % • Fibrohistiocytic pattern 20 % • Lymphovascular permeation	• Ki67 35 % • FISH for CDK4 –ve • FISH for MDM2 -ve
5 F/15	• Ca: 2.34 • PO_4: 1.21 • AP: 77	• Stromal and giant cell pattern • Moderate stromal cell nuclear pleomorphism	• Light brownish yellow firm tumor, 3 × 4 × 4.5 cm, left proximal tibial meta-epiphysis • Prominent hemorrhagic cystic and changes, focal cortical erosion but tumor confined to tibia	• Stromal and giant cell pattern 55 % • Aneurysmal cystic pattern 30 % • Fibrohistiocytic pattern 15 %	• Ki67: 39 % • FISH for CDK4 –ve • FISH for MDM2 -ve
6 F/31	• Ca: 2.38 • PO_4: 1.04 • AP: 64	• Stromal and giant cell pattern • Fibrohistiocytic pattern • Moderate stromal cell nuclear pleomorphism; lace-like osteoid	• Light yellowish fleshy tumor 5 × 5.9 × 7 cm replacing almost the entire right first metatarsal bone with focal cortical erosion and extension to soft tissue • Focal small areas of hemorrhages	• Stromal and giant cell pattern 70 % • Fibrohistiocytic pattern 30 %	• Ki67 37 % • FISH for CDK4 –ve • FISH for MDM2 -ve
7 M/11	• Ca: 2.36 • PO_4: 1.18 • AP: 362	• Trabecular and lace-like osteoid surrounded by osteoblast-like cells, mild nuclear pleomorphism • Many scattered osteoclastic cells	• Light brownish or yellowish gray firm to hard tumor 5.5 × 3 × 2.5 cm replacing almost the entire but confined to the right fourth metatarsal bone • Prominent hemorrhagic and cystic changes	• Stromal and giant cell pattern 55 % • Osteoblastoma-like pattern 30 % • Aneurysmal cystic pattern 10 % • Fibrohistiocytic pattern 5 %	• Ki67 33 % • FISH for CDK4 –ve • FISH for MDM2 -ve
8 M/15	• Ca: 2.35 • PO_4: 1.32 • AP: 140	• Stromal and giant cell pattern • Fibrohistiocytic pattern • Moderate stromal cell nuclear pleomorphism; lace-like osteoid	• Light grayish yellow soft to firm right distal femur metaphyseal tumor 3.5 × 4.5 × 7.5 cm • Prominent hemorrhagic cystic changes, focal cortical erosion forming Codman's triangle	• Stromal and giant cell pattern 60 % • Aneurysmal cystic pattern 20 % • Fibrous dysplasia-like pattern 15 % • Fibrohistiocytic pattern 5 %	• Ki67 36 % • FISH for CDK4 –ve • FISH for MDM2 -ve

Ca serum calcium, *PO_4* serum phosphate, *AP* serum alkaline phosphatase

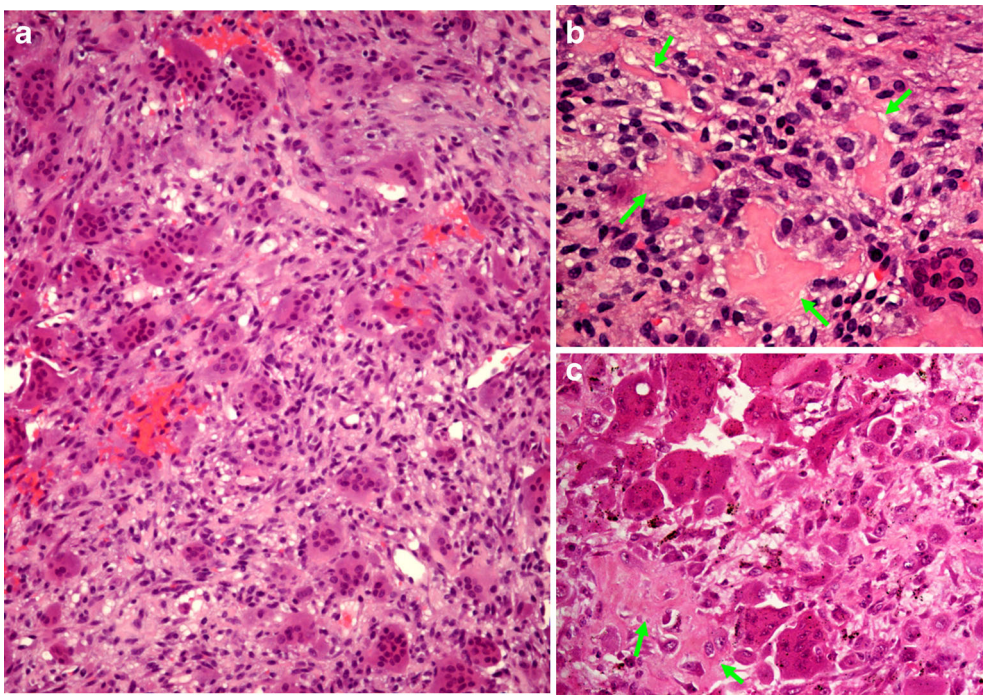

Fig. 4 **a** Biopsy histology of patient 5, showing a background of mononuclear stromal cells in which are many evenly distributed osteoclastic giant cells, supported in a fibrovascular stroma. (Hematoxylin and eosin, ×100) **b** Biopsy histology of patient 5. Some of the mononuclear stromal cells show moderate nuclear pleomorphism and hyperchromatism. Eosinophilic osteoid deposits are noted focally around the stromal cells (*arrows*). (Hematoxylin and eosin, ×200) **c** Resected tumor histology of patient 7. Eosinophilic lacelike osteoid deposits are noted focally around the moderately pleomorphic stromal cells (*arrows*) in this stromal and giant cell pattern. (Hematoxylin and eosin, ×200)

prominent nucleoli (Fig. 4b). There were focal irregular or lacelike osteoid deposits around stromal cells (Fig. 4b, c). This pattern was seen in all biopsies and accounted for over 50 % of the histology of all resected tumors.

Fibrohistiocytic pattern

In the fibrohistiocytic pattern, the mononuclear stromal cells were spindle-shaped and arranged in interlacing fascicules, focally assuming a storiform appearance (Fig. 5a, b). Scattered among these mononuclear cells were variable numbers of osteoclastic giant cells and metaplastic woven bone (Fig. 5b). Similar to the stromal and giant cell pattern, tumors bearing fibrohistiocytic appearances infiltrated into the surrounding native lamellar bony trabeculae (Fig. 5). Most stromal cells showed bland histologic features but in areas, they exhibited moderate to marked nuclear pleomorphism with focal irregular peri-cellular osteoid depositions (Fig. 5c, d). Such pattern was seen in all the biopsies and resected tumors.

Aneurysmal-cystic pattern

The microscopic aneurysmal-cystic pattern paralleled its macroscopic counterpart. The locules were of varying sizes, separated by fibrous septa of variable thickness (Fig. 6a, b). These septa consisted of an admixture of spindle or oval stromal cells, osteoclastic giant cells, small vessels and capillaries, extravasated red and inflammatory cells, siderophages and reactive woven bone, supported in a loose fibrous stroma (Fig. 6b, c). Some locules showed adherent fibrinous material and red cells on their surfaces (Fig. 6b). Most cells appeared benign; occasional septa focally harbored stromal cells with moderate nuclear pleomorphism, some surrounded by lacelike osteoid deposits (Fig. 6d). This form constituted more than 10 % of the tumor in five patients (62.5 %) but was seen as tiny fragments in two biopsies.

Osteoblastoma-like pattern

The resected tumor of patient 7 focally showed well circumscribed borders, consisting of a population of rather regular plump stromal cells with prominent osteoid or woven bone deposition in the form of interconnecting trabecular pattern, supported in a vascular stroma in which were evenly distributed osteoclastic giant cells. (Fig. 7a, b). The features resembled osteoblastoma but on high magnification, pericellular osteoid deposition around moderately to markedly pleomorphic cells with mitosis were noted (Fig. 7c). In small areas, the tumor show well-formed woven bony trabeculae in a background of loose fibroblastic stroma, indistinguishable from osteoblastoma (Fig. 7d). Such pattern was seen in the biopsy, in viable and coagulative necrotic forms admixed with other patterns throughout the post-chemotherapy specimen (Fig. 7e).

Parosteal and fibrous dysplasia-like pattern

Irregular woven bony trabeculae in parallel arrays embedded in a cellular fibroblastic stroma containing variable number of osteoclastic giant cells formed the parosteal and fibrous

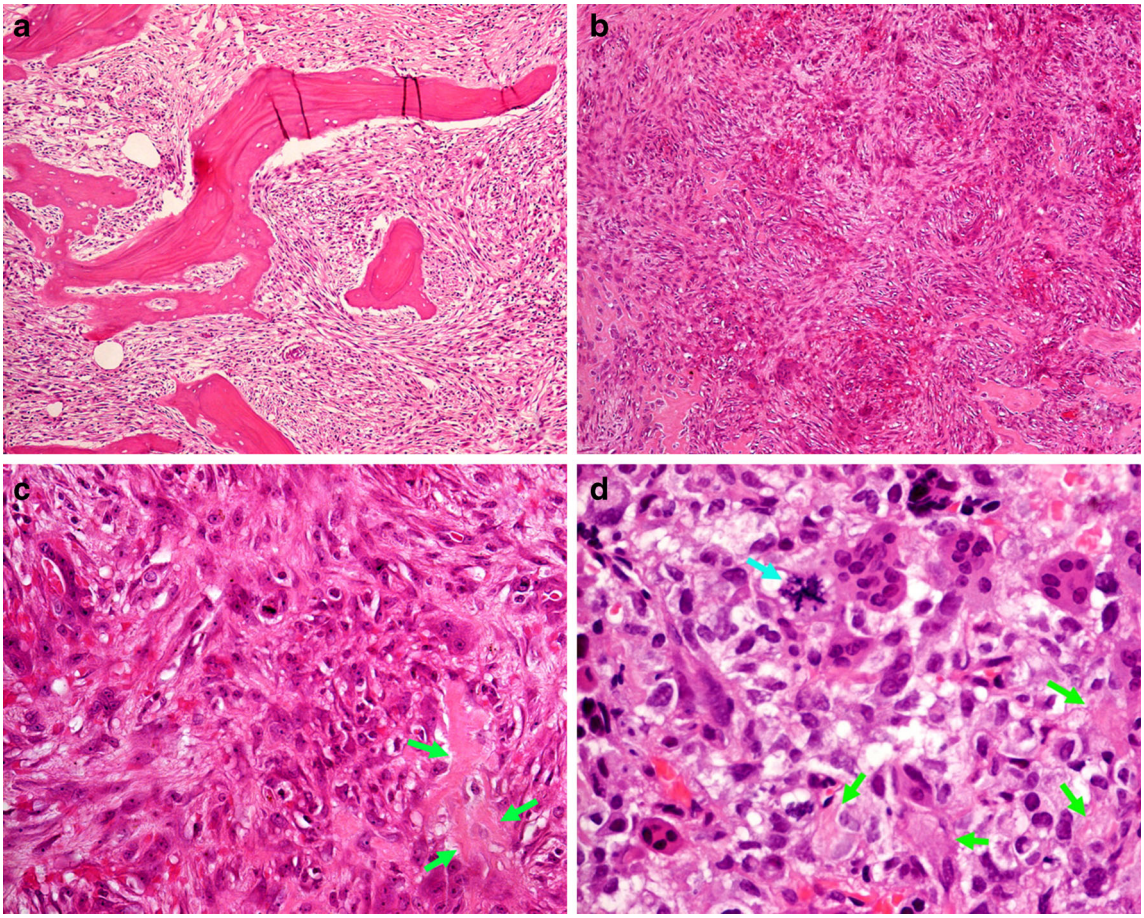

Fig. 5 **a** Resected tumor histology of patient 6. The mononuclear stromal cells assume spindle shape and are arranged in interlacing fascicles. Scattered among the stromal cells are some osteoclastic giant cells. The tumor infiltrates into surrounding native lamellar bony trabeculae. (Hematoxylin and eosin, ×40) **b** Resected tumor histology of patient 8. The interlacing fascicular stromal cells assume focally a storiform pattern. Among the stromal cells are variable number of osteoclastic giant cells and metaplastic woven bone. (Hematoxylin and eosin, ×100) **c** Resected tumor histology of patient 8. In areas of the fibrohistiocytic pattern, the mononuclear stromal cells show moderate nuclear pleomorphism and hyperchromatism. Lacelike osteoid deposition is noted focally around the stromal cells (*arrows*). (Hematoxylin and eosin, ×200) **d** Resected tumor histology of patient 8. Focal areas show atypical mitotic figure (*blue arrow*) and pleomorphic tumor cells with surrounding lacelike osteoid deposition (*green arrows*). (Hematoxylin and eosin, ×200)

dysplasia-like pattern (Fig. 8). The spindle fibroblastic cells showed mild pleomorphism with infrequent mitosis; in their midst were variable numbers of osteoclastic giant cells (Fig. 8b). Foci of anastomosing osteoid deposition around moderately pleomorphic plump oval stromal cells were present, reminiscent of membranous type ossification seen in parosteal and low grade central fibrous dysplasia-like osteosarcoma (Fig. 8c). Such pattern was noted in the periphery and randomly throughout the resected tumor of patient 8 but not in the biopsy.

CDK4 and MDM2 expression; Ki67 staining

CDK4 and MDM2 gene amplification was not detected in all seven cases examined. Immunohistochemical staining for CDK4 and MDM2 was completely negative in all the above histologic patterns. Ki67 staining was more than 30 % in the stromal and giant cell pattern in all cases and ranged from 20 to 30 % in the other patterns.

Histopathology in response to bisphosphonate and denosumab

In view of the giant cell-rich nature of the tumor, bisphosphonate alone and together with denosumab but no chemotherapy had been given prior to surgical resection in patients 2 and 6, respectively. Patient 3 received bisphosphonate, denosumab, and chemotherapy. Focal necrosis was seen in all three. In areas, mostly adjacent to necrotic foci, the osteoclastic giant cells were much fewer in number compared with the biopsy; the tumor consisted mostly of mononuclear stromal cells in a fibroblastic stroma. The two with concomitant denosumab administration showed broad woven bony trabeculae in the stroma (Fig. 8d).

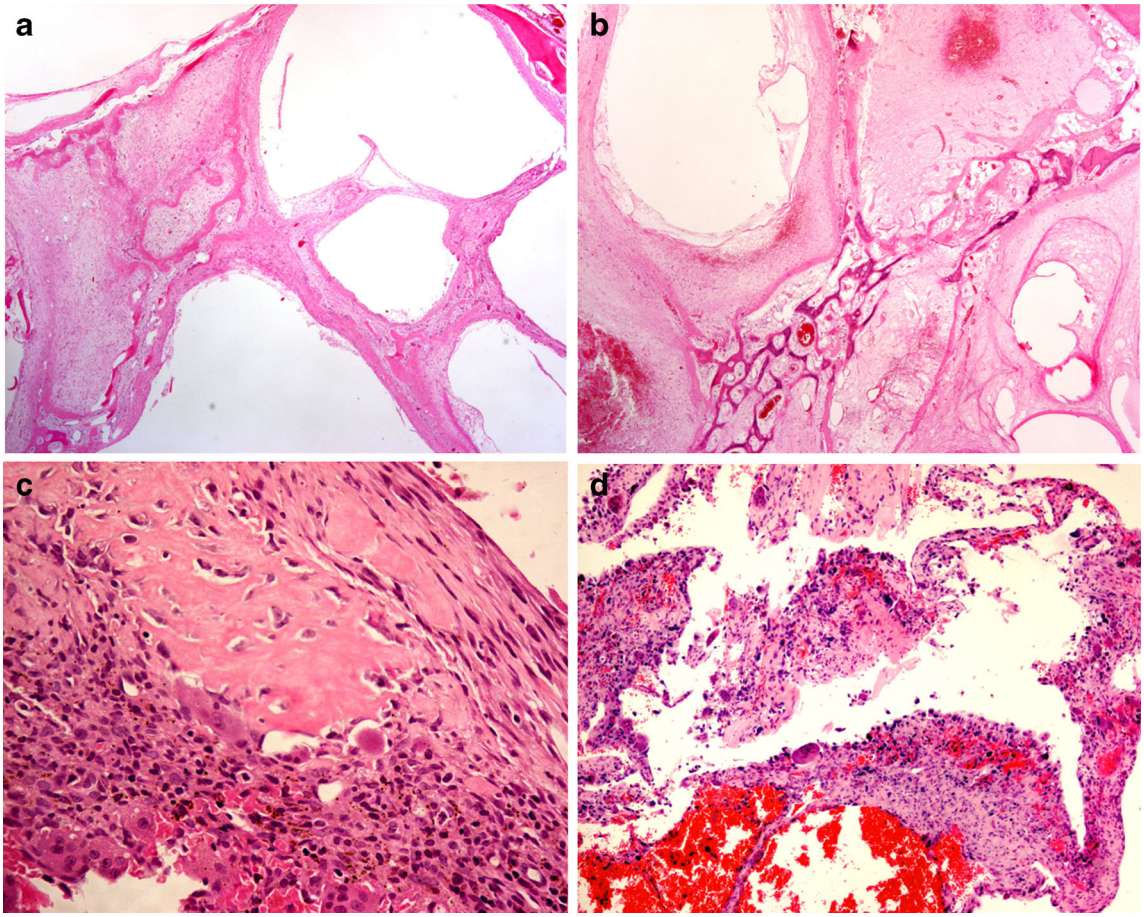

Fig. 6 **a** Resected tumor histology of patient 5. The aneurysmal cystic pattern consists of multiple locules of varying sizes separated by septa of variable thickness. (Hematoxylin and eosin, ×5) **b** Resected tumor histology of patient 5. The septa contain an admixture of stromal cells, vascular channels, extravasated red and inflammatory cells, and reactive woven bone supported in a loose fibrous stroma. Adherent on the surfaces of some of the locules are red cells and fibrinous material (Hematoxylin and eosin, ×10) **c** Resected tumor histology of patient 3. In the septa is focal reactive woven bone formation in the midst of oval or spindle stromal and osteoclastic giant cells. There are extravasated red and inflammatory cells. (Hematoxylin and eosin, ×100) **d** Resected tumor histology of patient 1. Occasional septa appear cellular and consist of mainly an admixture of stromal and osteoclastic giant cells. Some stromal cells show moderate to marked nuclear pleomorphism and are surrounded by lacelike osteoid deposits (Hematoxylin and eosin, ×100)

Treatment and outcome

Patients 2 and 3 were treated initially by curettage and local resection, respectively, due to initial diagnosis of GCT. Despite subsequent chemotherapy, both pursued aggressive clinical course and died 14 and 21 months after presentation. Amputation was required for patient 1 due to skip metastasis while the others underwent local resection after chemotherapy; they remained well 12 to 110 months after presentation.

Discussion

Defining GCRO

Bathurst used the term "osteoclast-rich osteosarcoma" to denote "an undifferentiated sarcoma with scanty or no tumor osteoid, in which the sarcoma cells are more or less swamped by osteoclasts producing a striking resemblance to a GCT". Osteosarcomas rich in osteoclasts but with abundant osteoid or chondroid matrix have been excluded whereas one with no tumor osteoid has been accepted as osteosarcoma [2]. The defects of such definition include the lack of indication on the quantity of giant cell-rich areas required for such designation, the illogical exclusion of osteosarcomas rich in both osteoclastic giant cells and osteoid, and most importantly the desertion of the requirement of osteoid deposition around tumor cells as the basic definition for osteosarcoma. In this manner, giant cell undifferentiated pleomorphic sarcoma of bone would awkwardly be regarded as GCRO. Although Shuhaibar recognized the lack of accurate definition for GRCO which in their opinion should be reserved for "those osteosarcomas that contain an abundance of osteoclast-like giant cells distributed throughout the tumor" [12] but their own reported case represented a unique parosteal osteosarcoma which at presentation showed dedifferentiation to GCRO.

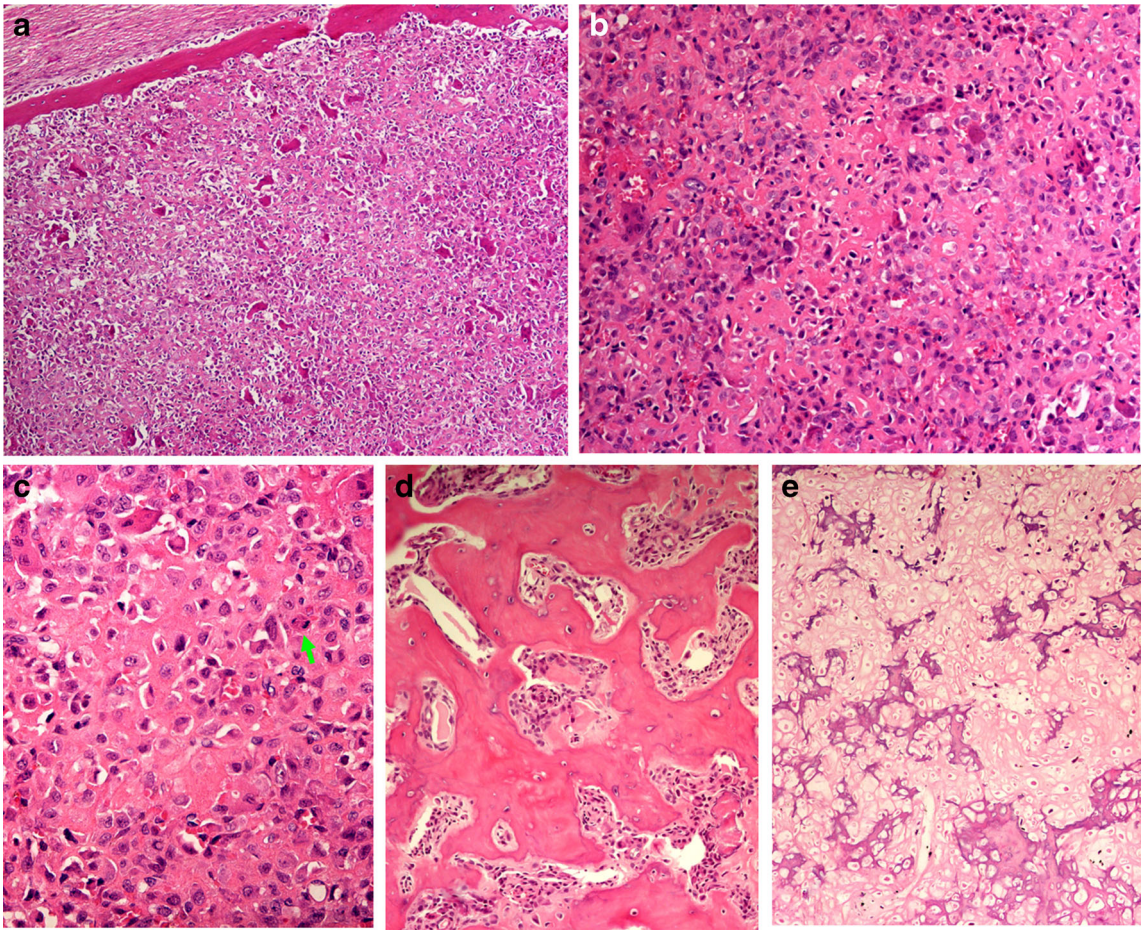

Fig. 7 **a** Resected tumor histology of patient 7. The tumor in areas exhibits a well circumscribed and pushing border and consists of a population of rather regular plump stromal cells showing prominent osteoid or woven bone deposition in the form of interconnecting uniform trabecular pattern and supported in a vascular stroma in which were fairly evenly distributed osteoclastic giant cells. The low power features resemble those of osteoblastoma (Hematoxylin and eosin, ×40) **b** Resected tumor histology of patient 7. The osteoblastoma like pattern consists of a population of rather regular plump stromal cells showing prominent osteoid or woven bone deposition in the form of interconnecting uniform trabecular pattern and supported in a vascular stroma in which were fairly evenly distributed osteoclastic giant cells. (Hematoxylin and eosin, ×100) **c** Resected tumor histology of patient 7. The tumor cells in the osteoblastoma like pattern exhibit moderate nuclear pleomorphism, exhibit mitosis (*arrow*), and are surrounded by lacelike osteoid. (Hematoxylin and eosin, ×200) **d** Resected tumor histology of patient 7. In small areas, the tumor shows focal well-formed woven bony trabeculae in a background of loose fibrovascular stroma, virtually indistinguishable from osteoblastoma. (Hematoxylin and eosin, ×200) **e** Resected tumor histology of patient 7. The tumor exhibits focal coagulative necrosis after chemotherapy. The regularity of the tumor cells and the prominent osteoid and woven bone formation around individual and clusters of cells are more clearly demonstrated. (Hematoxylin and eosin, ×200)

Thus, "it shows several histological patterns. Some areas show pleomorphic spindle cells, abundant osteochondroid matrix, and scattered osteoclast-like giant cells. Other areas are composed of sheets of osteoclast-like giant cells in a background of mononuclear cells with numerous mitoses (up to two per high-power field, ×40 objective)" representing the GCRO component [12]. Accordingly, the requirement of "an abundance of osteoclast-like giant cells distributed throughout the tumor" would be too restrictive and not in harmony with the criteria in the conventional histologic subtyping of osteosarcoma.

Associated with this absence of precise defining criteria for GRCO is the lack of detailed characterization of its histologic features. Most GCRO is depicted as many osteoclastic giant cells distributed among oval tumor cells with scanty, coral-like, lacy osteoid formation [5], with little reference to its gross and remaining histologic appearance. By incorporating into our definition of GCRO explicitly, the defining histologic features of GCT, specifying quantitatively it being the dominating component according to convention, and the tumor is an unequivocal osteosarcoma; the drawbacks in Bathurst's definition are removed.

Clinical and radiologic features

The clinical presentations, initial radiologic, and pathologic diagnoses and outcomes of all reported cases including the present series are summarized in Table 3.

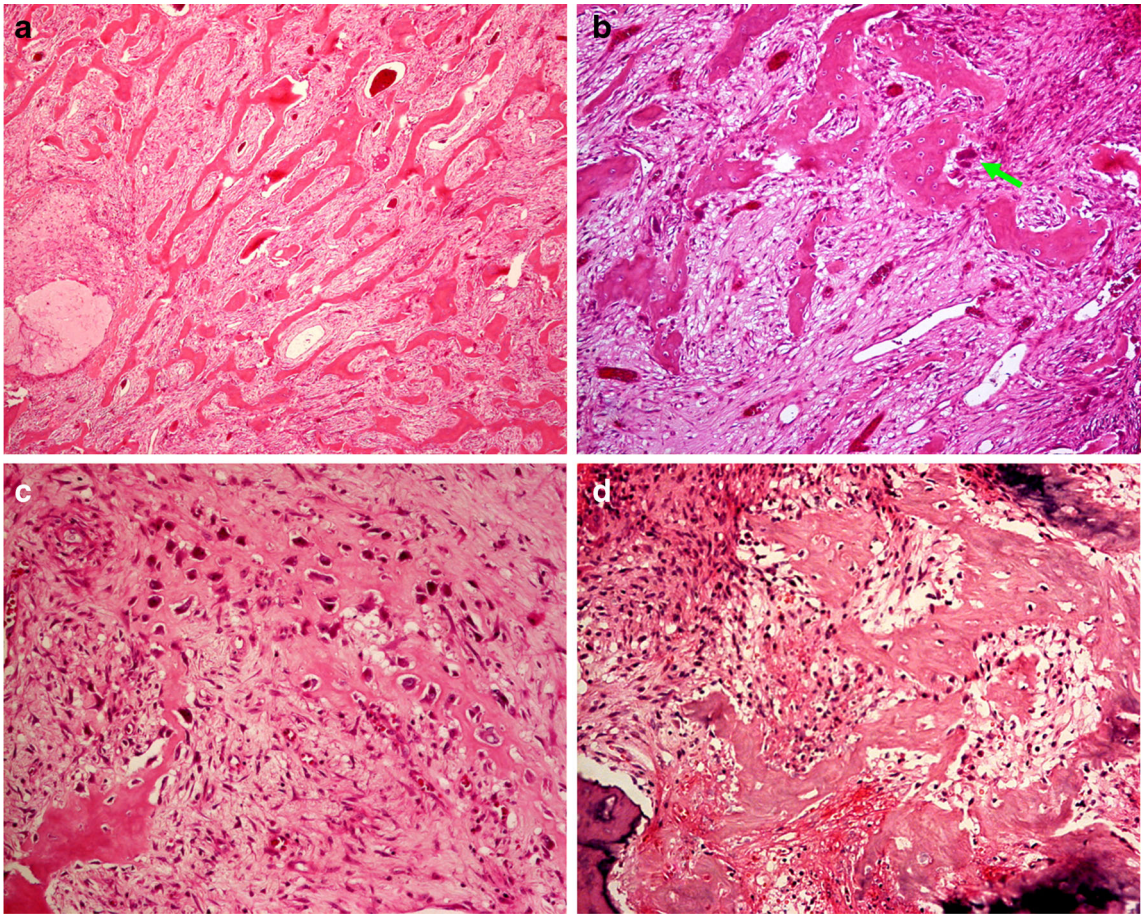

Fig. 8 **a** Resected tumor histology of patient 8. The parosteal and fibrous dysplasia like pattern consists of irregular woven bony trabeculae focally arranged in small parallel arrays in a background of cellular fibroblastic stroma. (Hematoxylin and eosin, ×40) **b** Resected tumor histology of patient 8. The parosteal and fibrous dysplasia like pattern consists of irregular woven bony trabeculae in a background of cellular fibroblastic stroma. The spindle stromal cells show mild cellular pleomorphism and in their midst are some osteoclastic giant cells (*arrow*). (Hematoxylin and eosin, ×100) **c** Resected tumor histology of patient 8. Small foci of anastomosing osteoid deposition around mildly to moderately pleomorphic plump oval stromal cells are present, reminiscent of membranous type ossification seen in parosteal and low grade central fibrous dysplasia like osteosarcoma. (Hematoxylin and eosin, ×200) **d** Resected tumor histology of patient 3. Focally, the tumor consists mostly of mononuclear stromal cells embedded in a fibroblastic stroma in which broad woven bony trabeculae are noted. The osteoclastic giant cells are much reduced in number as compared with that in the biopsy. (Hematoxylin and eosin, ×200)

GCRO accounts for 3.02 % (8/265) of all osteosarcomas in our institution, comparable to the 3 and 2.99 % reported by Bathurst and Wang, respectively [2, 5]. The clinical characteristics are in accordance to the culminated data. The patient' age range from 6 to 67 years [2, 20], peak incidence between 11 and 20, male to female ratio 1.28. The majority (37/41 = 90 %) presents with pain lasting from a few weeks to months, the three exceptions are the patients with metatarsal, tibial, and maxillary GCRO complaining of enlarging masses for 2, 2, and 5 years, respectively [3, 5, 21]. Most (24/41 = 58.5 %) occurs in the knee region, the femur (17/41 = 41.5 %), and tibia (14/41 = 34.1 %). In the long bones, GCRO is commonly metaphyseal (22/35 = 62.9 %) in location, followed by diaphyseal (9/35 = 25.7 %) and epiphyseal (4/35 = 11.4 %). The clinical features of GCRO are thus similar to conventional high-grade osteosarcoma apart from its more common diaphyseal location. Another difference is the normal serum bone-specific alkaline phosphatase levels in all our cases, reflecting its scant osteoid and bone formation.

Besides the characteristic radiographic appearances of expansile osteolytic lesions with variable degrees of cortical erosion, periosteal reaction, and absence of osteoblastic areas [2–5], our GCRO shows a higher percentage of well-circumscription and multiloculations; MRI reveals internal septa with multiloculations and multiple fluid levels in 62.5 % (Tables 1 and 3). Such features reflect the close similarities between GCRO and GCT with regard to gross and histomorphology. GCRO has thus been mistaken radiologically as GCT in 62.5 % of our cases compared with 36.4 % (12/33) of the others (Table 3). The probable explanation is our more structured definition of GCRO results in selection of tumors bearing greater resemblance to GCT while some

Table 3 Summary of the clinical, radiologic, and pathologic characteristic of the reported case of giant cell rich osteosarcoma

Sex	Age (years)	Location	Symptoms	Radiologic Dx	Initial pathologic Dx	Outcome
Bathurst [2] 9 cases M:F = 5:4	1–10: 2 11–20: 5 21–30: 1 31–40: 1	• Femur diaphysis-5 • Femur epiphysis-1 • Tibia metaphysis-2 • Tibia diaphysis-1	Pain ± LOM-4 Painful mass-5	Aneurysmal bone cyst-2 Giant cell tumor-2 Osteosarcoma-2 Fibrosarcoma-1 CMF-1 Ewing's sarcoma-1	Not stated	DWD-4 (24–36 months) NED-5 (12–192 months)
Wang [5] 9 cases M:F = 5:4	11–20: 5 21–30: 0 31–40: 3 41–50: 1	• Tibia metaphysis-7 • Femur metaphysis-2	Pain ± LOM-6 Painful mass-3	Giant cell tumor-6 Osteosarcoma-1 Malignant tumor-1 Possibly osteosarcoma-1	GCRO-6 Giant cell tumor-3	DWD-3 (13–20 months) AWD-1 (5 months) NED-5 (74–114 months)
Case reports [7–21] 15 cases M:F = 9:6	11–20: 5 21–30: 5 31–40: 2 40–50: 0 51–60: 2 61–70: 1	• Femur metaphysis-4 • Femur diaphysis-3 • Tibia metaphysis-2 • Fibula epiphysis-1 • Radius epiphysis-1 • Tarsal navicular bone-1 • Rib-1 • Mandible/maxilla-2	Pain ± LOM-7 Painful mass-5 Painless mass-2 Pathologic #-1	Osteosarcoma-8 Giant cell tumor-4 Parosteal osteosarcoma-2 Aneurysmal bone cyst-1	Giant cell tumor-8 GCRO-5 Osteosarcoma-1 GCRG-1	DWD-2 (41–237 moths) NED-8 (11–72 months) Unavailable-5
Present study 8 cases M:F = 4:4	11–20: 4 21–30: 2 31–40: 2	• Femur metaphysis-2 • Femur epiphysis-1 • Metatarsal bone-2 • Tibia metaphysis-2 • Fibula metaphysis-1	Pain ± LOM-3 Painful mass-4 Pathologic #-1	Giant cell tumor ± ABC-5 Osteosarcoma-2 Possibly osteosarcoma-1	GCRO-5 Osteosarcoma-2 Giant cell tumor-1	DWD-2 (14–21 moths) NED-6 (12–110 months)
All 41 cases M:F = 23:18	1–10: 2 11–20: 19 21–30: 8 31–40: 8 41–50: 1 51–60: 2 61–70: 1	• Femur metaphysis-8 • Femur diaphysis-8 • Femur epiphysis-1 • Tibia metaphysis-13 • Tibia diaphysis-1 • Fibula epiphysis-2 • Fibula metaphysis-1 • Radius epiphysis-1 • Metatarsal-2 • tarsal navicular bone-1 • Rib-1 • Mandible/maxilla-2	Pain ± LOM-20 Painful mass-17 Painless mass-2 Pathologic #-2	Giant cell tumor-17 Osteosarcoma-13 Aneurysmal bone cyst-3 Parosteal osteosarcoma-2 Possibly osteosarcoma-2 Fibrosarcoma-1 Ewing's sarcoma-1 Malignant tumor-1 CMF-1	GCRO-16 Giant cell tumor-12 Osteosarcoma-3 GCRG-1	DWD-11 (13–237 moths) AWD-1 (5 months) NED-24 (11–192 months) Unavailable-5

Dx diagnosis, *LOM* limitation of movement, *GCRO* giant cell rich osteosarcoma, *DWD* death with disease, *AED* alive with disease, *NED* no evidence of disease, *M* male, *F* female, # fracture, *ABC* aneurysmal bone cyst, CMF chondromyxoid fibroma,*GCRG* giant cell reparative granuloma

reported cases may contain a higher proportion of high-grade osteosarcomatous component, leading to more aggressive radiologic appearances.

Histopathology

As the defining pattern for GCRO, the stromal and giant cell, present in all cases, makes up 55 to 80 % of the tumor. While present in all cases, the fibrohistiocytic pattern prevails in cases where the aneurysmal-cystic pattern is absent. Tumor cells in these two patterns typically show mild nuclear pleomorphism with infrequent mitosis but, focally, they assume moderate to marked pleomorphism and are surrounded by lacelike osteoid deposits. This feature allows its differentiation from GCT sometimes even in needle biopsies.

The aneurysmal-cystic pattern constitutes more than 10 % of the tumors in 62.5 % and gives them their characteristic multiloculated gross and radiological appearances, overlapping with GCT. Most appear benign, representing secondary aneurysmal bone cysts. However, few septa show osteosarcomatous features and lead Bathurst to suggest GCRO may be a solid variant of telangiectatic osteosarcoma [2]. This postulation is unsubstantiated by our finding of additional histologic components in GCRO but not in telangiectatic osteosarcoma.

Osteoblastoma-like, parosteal and fibrous dysplasia-like osteosarcomas are low grade variants, each accounting for about 1 % of all osteosarcomas [27, 28]. The parosteal and fibrous dysplasia-like osteosarcomatous component has been described in high-grade osteosarcoma and interpreted as dedifferentiation [26]. A patient with GCRO resulting from dedifferentiated parosteal osteosarcoma at presentation has been reported [12]. The parosteal GCRO reported by Sciot shows radiologic, gross, and histopathologic features typical

of parosteal osteosarcoma but the stromal and giant cell pattern is also a dominating feature [10]. Such phenomenon has not been described for osteoblastoma-like osteosarcoma. Our two cases are unique in the occurrence of these two low-grade osteosarcoma patterns as part of the GCRO. Their intimate admixture with other histologic especially the stromal and giant cell patterns throughout the entire tumor and the short clinical symptoms are against the process of dedifferentiation. They most probably represent constituting components of GCRO.

While the stromal and giant cell, fibrohistiocytic and aneurysmal-cystic patterns may be seen in GCRO and GCT, the osteoblastoma-like and parosteal and fibrous dysplasia-like patterns are absent in the latter. Of prime importance is the focal subtle lacelike pericellular osteoid deposition and permeative infiltration that distinguish GCRO from GCT, finally the stromal and giant cell pattern exceeding 50 % establishes the diagnosis of GCRO.

CDK4 and MDM2 expression; Ki67 staining

While 89 % of fibrous dysplasia-like and parosteal osteosarcomas show CDK4 and MDM2 amplification [25], none is seen in our seven GCRO, in all patterns including the osteoblastoma-like and parosteal and fibrous dysplasia-like areas. Acknowledging the limitations of small sample size especially the single cases for low-grade areas, it appears logical to conclude that GCRO typically lacks CDK4 and MDM2 amplification, in keeping with its many clinical similarities to high-grade osteosarcoma.

Ki67 proliferative index is high in all GCRO, over 30 % in the stromal and giant cell pattern, and range from 20 to 30 % in the others. As analyzed previously, such high Ki67 proliferative index in giant cell-rich tumors probably denotes an aggressive potential [3].

Histopathology in response to bisphosphonate and denosumab

As bisphosphonate and denosumab is beneficial for GCT [29], they have been given, singly or in combination, preoperatively to three: patient 2 with initial diagnosis of GCT, patients 3 and 6, probably GCRO diagnosed by needle biopsy, in an attempt to consolidate the tumor. Bisphosphonate binds to bone surfaces where after assimilation by osteoclasts inhibits farnesyl diphosphate synthase, disrupting their resorptive function [30]. This is manifested histologically by "giant osteoclasts" containing many pyknotic nuclei detaching from bone surfaces [31]. Denosumab as a RANK ligand inhibitor reduces and replaces RANK-positive tumor stromal and giant cells by woven bone [32]. The lack of clinical response is reflected by the absent bisphosphonate-induced histology with no giant osteoclasts; there is only focal tumor necrosis and reduction in osteoclastic giant cells. The two receiving additional denosumab treatments show focal broad trabecular woven bone formation, suggestive limited denosumab-induced effects. Our three-case trial therefore suggests the lack of benefits of bisphosphonate and denosumab in GCRO.

Remarkably, Wojcik highlighted the morphologic alterations of denosumab-treated GCT that may lead to its confusion with osteosarcoma [33]. When treatment lasts for 2–8 months, the lesions are highly cellular, with cellular atypia and haphazard bone deposition, resulting in their resemblance to high-grade osteosarcoma. The minor degree of atypia, infrequent mitosis, and lack of permeative growth pattern allow their distinction from high-grade osteosarcoma. After therapy for 19–55 months, the reduced cellularity and new bone deposition as long curvilinear arrays mimic low-grade osteosarcomas from which they can be distinguished by the lack of infiltrative growth and negative CDK4 and MDM2 staining.

Clinical course

All our patients present with Enneking stage 1A disease; two die from disseminated metastasis 14 and 21 months after presentation but their initial treatments are inappropriate. The others survive; however, most of their follow-up periods are short. Admitting the small number of cases, incomplete data from case reports, and lacking stringent statistical analysis, our results appear comparable to Wang [5] and the culminated data. Besides, the survival rate may not differ much from high-grade osteosarcoma, 60–70 % at 5 years [34].

Conclusion

By defining GCRO as "*an osteosarcoma in which more than 50% of the tumor consists of numerous uniformly distributed osteoclastic giant cells amidst oval or spindle mononuclear cells embedded in a fibrovascular stroma*", thereby eliminating those conventional high grade osteosarcoma with mere focal giant-cell rich areas, several distinctive radiologic and histologic features of a more homogeneous population of GCRO are identified. The similarities between GCRO and GCT extend beyond the histologic appearances of the stromal and giant cell pattern, propensity of fibrohistiocytic and aneurysmal cystic formation to the radiologic features of expansile nature yet relatively well circumscription, focal cortical erosion, and multiloculations. GCRO distinguishes itself from GCT by the histologic hallmark of definite though focal and subtle lacelike osteoid deposition around moderately to markedly pleomorphic tumor cells, permeative infiltration into adjacent native bony trabeculae, occasional association with osteoblastoma-like, parosteal and fibrous dysplasia-like or possibly other osteosarcomatous pattern, high KI67 proliferative index, and radiologically more frequent periosteal

reaction. GCRO accounts for about 3 % of all osteosarcomas, and apart from its more frequent diaphyseal location and associated normal bone-specific alkaline phosphate levels, it shares with conventional high-grade osteosarcoma the same patient demographics, sites of occurrence, absence of CDK4 and MDM2 amplification, and probably clinical course.

Compliance with ethical standards The author declares that the study complies with the ethical standards required.

Funding The author declares no funding received for this work.

Conflict of Interest The author declares that they have no competing interests.

References

1. Klein MJ, Siegal GP (2006) Osteosarcoma: anatomic and histologic variants. Am J Clin Pathol 125:555–581
2. Bathurst N, Sanerkin N (1986) Watt I Osteoclast-rich osteosarcoma. Br J Radiol 59:667–673
3. Chow LTC (2015) Fibular giant cell-rich osteosarcoma virtually indistinguishable radiographically and histopathologically from giant cell tumor—analysis of subtle differentiating features. APMIS 123(6):530–539
4. Chow LTC, Wong SKC (2015) Epiphyseal osteosarcoma revisited: four illustrative cases with unusual histopathology and literature review. APMIS 123(1):9–17
5. Wang CS, Yin QH, Liao JS, Lou JH, Ding XY, Zhu YB (2013) Giant cell-rich osteosarcoma in long bones: clinical, radiological and pathological features. Radiol Med. 118(8):1324–1334. doi:10.1007/s11547-013-0936-9 Epub 2013 May 27
6. Fletcher CDM, Bridge JA, Hogendoorn P, Mertens F (2013) WHO Classification of tumours of soft tissue and bone, Fourth Edition., World Health Organization classification of tumors, vol Volume 5. IARC Press, Lyon, France, pp. 282–288
7. Rietveld LAC, Mulder JD, de la Rivière G B, van Rijssel TG (1981) Giant cell tumour: metaphyseal or epiphyseal origin? Diagn Imaging 50(6):289–293
8. Picci P, Manfrini M, Zucchi V, Gherlinzoni F, Rock M, Bertoni F, Neff JR (1983) Giant-cell tumor of bone in skeletally immature patients. J Bone Joint Surg Am 65(4):486–490
9. Kransdorf MJ, Sweet DE, Buetow PC, Giudici MA, Moser RP Jr (1992) Giant cell tumor in skeletally immature patients. Radiology 184(1):233–237
10. Sciot R, Samson I, Dal Cin P, Lateur L, van Damme B, van den Berghe H, Desmet V (1995) Giant cell rich parosteal osteosarcoma. Histopathology 27(1):51–55
11. Sato K, Yamamura S, Iwata H, Sugiura H, Nakashima N, Nagasaka T (1996) Giant cell-rich osteosarcoma: a case report. Nagoya J Med Sci 59(3–4):151–157
12. Shuhaibar H, Friedman L (1998) Dedifferentiated parosteal osteosarcoma with high-grade osteoclast-rich osteogenic sarcoma at presentation. Skelet Radiol 27(10):574–577
13. Sundaram M, Totty WG, Kyriakos M, McDonald DJ, Merkel K (2001) Imaging findings in pseudocystic osteosarcoma. Am J Roentgenol 176(3):783–788
14. Bertoni F, Bacchini P, Staals EL (2003) Giant cell-rich osteosarcoma. Orthopedics 26(2):179–181
15. Shinozaki T, Fukuda T, Watanabe H, Takagishi K (2004) Giant cell-rich osteosarcoma simulating giant cell tumor of bone. Kitakanto Med J 54:147–151
16. Hong SJ, Kim KA, Yong HS, Choi JW, Suh SI, Lee JH, Shon WY (2005) Giant cell-rich osteosarcoma of bone. Eur J Radiol Extra 53:87–90
17. Nagata S, Nishimura H, Uchida M, Hayabuchi N, Zenmyou M, Harada H (2006) Giant cell-rich osteosarcoma of the distal femur: radiographic and magnetic resonance imaging findings. Radiat Med 24(3):228–232
18. Kinoshita G, Yasoshima H (2006) Giant cell-rich tumor of the rib. J Orthop Sci 11(3):312–317
19. Gambarotti M, Donato M, Alberghini M, Vanel D (2011) A strange giant cell tumor. Eur J Radiol 77(1):3–5. doi:10.1016/j.ejrad.2010.06.050
20. Fu HH, Zhuang QW, He J, Wang LZ, He Y (2011) Giant cell-rich osteosarcoma or giant cell reparative granuloma of the mandible? J Craniofac Surg 22(3):1136–1139. doi:10.1097/SCS.0b013e3182108fbf
21. Verma RK, Gupta G, Bal A, Yadav J (2011) Primary giant cell rich osteosarcoma of maxilla: an unusual case report. J Maxillofac Oral Surg 10(2):159–162. doi:10.1007/s12663-010-0066-z Epub 2011 Mar 25
22. Imran AA, Khaleel ME, Salaria SM, Hasan M (2012) Giant cell-rich osteosarcoma: unravelling an elusive, enigmatic entity. Int J Pathol 10(1):36–38
23. Kinra P, Valdamani S, Singh V, Dutta V (2012) Diaphyseal giant cell-rich osteosarcoma: unusual histological variant in an unusual site. Indian J Pathol Microbiol 55(4):600–602. doi:10.4103/0377-4929.107848
24. Mariano FV, Corrêa MB, da Costa MV, de Almeida OP, Lopes MA (2013) Labial mucosa metastasis of fibule giant cell-rich osteosarcoma: an unusual presentation. Quintessence Int 44(10):783–791. doi:10.3290/j.qi.a29609
25. Dujardin F, Binh MB, Bouvier C, Gomez-Brouchet A, Larousserie F, Muret A, Louis-Brennetot C, Aurias A, Coindre JM, Guillou L, Pedeutour F, Duval H, Collin C, de Pinieux G (2011) MDM2 and CDK4 immunohistochemistry is a valuable tool in the differential diagnosis of low-grade osteosarcomas and other primary fibro-osseous lesions of the bone. Mod Pathol 24(5):624–637. doi:10.1038/modpathol.2010.229
26. Yoshida A, Ushiku T, Motoi T, Beppu Y, Fukayama M, Tsuda H, Shibata T (2012) MDM2 and CDK4 immunohistochemical coexpression in high-grade osteosarcoma: correlation with a dedifferentiated subtype. Am J Surg Pathol 36(3):423–431. doi:10.1097/PAS.0b013e31824230d0
27. Bertoni F, Bacchini P, Donati D, Martini A, Picci P, Campanacci M (1993) Osteoblastoma-like osteosarcoma. The Rizzoli Institute experience. Mod Pathol 6(6):707–716
28. Kurt AM, Unni KK, McLeod RA, Pritchard DJ (1990) Low-grade intraosseous osteosarcoma. Cancer 65(6):1418–1428
29. Tse LF, Wong KC, Kumta SM, Huang L, Chow TC, Griffith JF (2008) Bisphosphonates reduce local recurrence in extremity giant cell tumor of bone: a case-control study. Bone 42(1):68–73 Epub 2007 Sep 6
30. Fisher JE, Rodan GA, Reszka AA (2000) In vivo effects of bisphosphonates on the osteoclast mevalonate pathway. Endocrinology 141(12):4793–4796
31. Jobke B, Milovanovic P, Amling M, Busse B (2014) Bisphosphonate-osteoclasts: changes in osteoclast morphology and function induced by antiresorptive nitrogen-containing bisphosphonate treatment in osteoporosis patients. Bone 59:37–43. doi:10.1016/j.bone.2013.10.024 Epub 2013 Nov 6
32. Branstetter DG, Nelson SD, Manivel JC, Blay JY, Chawla S, Thomas DM, Jun S, Jacobs I (2012) Denosumab induces tumor reduction and bone formation in patients with giant-cell tumor of

bone. Clin Cancer Res 18(16):4415–4424. doi:10.1158/1078-0432.CCR-12-0578 Epub 2012 Jun 18

33. Wojcik J, Rosenberg AE, Bredella MA, Choy E, Hornicek FJ, Nielsen GP, Deshpande V (2016) Denosumab-treated giant cell tumor of bone exhibits morphologic overlap with malignant giant cell tumor of bone. Am J Surg Pathol 40(1):72–80. doi:10.1097/PAS.0000000000000506
34. Mirabello L, Troisi RJ, Savage SA (2009) Osteosarcoma incidence and survival rates from 1973 to 2004: data from the Surveillance, Epidemiology, and End Results Program. Cancer 115(7):1531–1543. doi:10.1002/cncr.24121